



Spin Tracking with Siberian Snakes in RHIC

M. Xiao^a and T. Katayama^b

^aFermi National Laboratory, Batavia, IL, 60510, USA

^bCenter for Nuclear Study, Graduate School of Science, the University of Tokyo,
Wako, Hirosawa 2-1, Japan

1 Introduction

The Relativistic Heavy Ion Collider (RHIC) at Brookhaven National Laboratory has the unique capability of colliding polarized proton beams with $\sqrt{s} = 500$ GeV. To achieve collision of such high energy polarized proton beams, polarization needs to be preserved during acceleration from injection energy (25 GeV) to top energy (250 GeV). This is accomplished by using Siberian Snakes - local spin rotators conceived by Derbenev and Kondratenko in 1988 [1] - to suppress spin depolarization resonances. For the RHIC-Spin Project, installation of two Siberian Snakes in the main rings was planned. Each snake is composed of four superconducting helical dipole magnets and generates 180° of spin rotation about the horizontal axis. The behavior of spin precession and orbital motion of protons, including the effects of Siberian Snakes [2, 3] and the strengths of spin resonance of intrinsic and imperfection type have been extensively studied both analytically and numerically. In those studies, the magnetic fields of helical magnets is approximated by an analytical model due to Blewett and Chasman [4]. Not surprisingly, real helical dipole magnets differ somewhat from this idealized model: they exhibit a non-negligible longitudinal magnetic field and fringing fields at both entrance and exit extremities. In 1997, magnetic field measurements on a prototype helical magnet showed excellent agreement with numerical calculations performed with the three-dimensional magnetostatics code TOSCA[5]. This result suggested that it should be possible to perform reliable numerical study of spin motion by tracking orbital and spin motion around the ring using numerically generated Snake magnetic field maps.

In the present paper, we obtain energy-dependent numerical orbital maps and spin matrices of a Siberian Snake, from injection to top energy. A technique based on spline interpolation functions is used to construct a suitably smooth field map. TPSA (Truncated

Power Series Algebra or Automatic Differentiation) is subsequently employed to produce an orbital map. Since tracking involves in excess of 10^7 turns, symplecticity must be enforced and we describe how this can be accomplished. Finally, results of spin tracking in the presence of Siberian Snakes are presented and discussed.

2 Spin Matrices and Orbital Maps of Siberian Snakes

The evolution of spin vector of polarized protons in external electromagnetic fields is governed by the Thomas – BMT equation [6]. Spin precession depends on the ambient magnetic field and thus is coupled with the orbital motion, which obeys the Lorentz equation. In Frenet-Serret coordinates system, the equations of orbital motion are given as follows:

$$\begin{aligned}
 \frac{ds}{ds} &= 1, \\
 \frac{dx}{ds} &= x' = u \\
 \frac{dy}{ds} &= y' = v \\
 \frac{du}{ds} &= w \cdot [uvB_x - (1+u^2)B_y + vB_s] \\
 \frac{dv}{ds} &= w \cdot [(1+v^2)B_x - uvB_y + uB_s]
 \end{aligned} \tag{2.1}$$

where $w = \frac{e \cdot \sqrt{1+u^2+v^2}}{m_o \gamma \mathcal{V}}$ and V is the velocity of a charged particle. B_x , B_y and B_s are the components of magnetic field in x , y and s directions, respectively. In the same coordinate system, the Thomas – BMT equation is [7];

$$\frac{d\vec{S}}{ds} = \vec{S} \times \vec{P}, \tag{2.2}$$

where \vec{S} is the spin vector and $\vec{P} = (P_x, P_y, P_s)$ depends on the three components of the magnetic field and the particle coordinates;

$$P_x = \frac{\hbar}{B\rho} \cdot \left\{ (1+G\gamma)[(1+v^2)B_x - uvB_y - uB_s] + (1+G)u(uB_x + vB_y + B_s) \right\} \tag{2.2a}$$

$$P_y = \frac{h}{B\rho} \cdot \left\{ (1 + G\gamma)[(1 + u^2)B_x - uvB_y - vB_s] + (1 + G)v(uB_x + vB_y + B_s) \right\} \quad (2.2b)$$

$$P_s = \frac{h}{B\rho} \cdot \left\{ (1 + G\gamma)[(-uB_x - vB_y + (u^2 + v^2)B_s)] + (1 + G)(uB_x + vB_y + B_s) \right\} \quad (2.2c)$$

with $h = (1 + u^2 + v^2)^{1/2}$, $B\rho = m_o\gamma V / e$, $V \equiv |\vec{v}|$.

In principle, assuming either a measured or a numerically obtained field map, straightforward Runge-Kutta quadrature can be used to integrate Eq.(2.1) and Eq.(2.2). An orbital map and a spin matrix can then be extracted. TPSA (Truncated Power Series Algebra or Automatic Differentiation) approach [8] permits the calculation of a truncated Taylor map of an arbitrary element to any order and the Taylor coefficients of the resulting truncated map will be accurate to the precision of computer. In order to make use of the TPSA approach in the present study, the numerical magnetic field was fitted with spline functions, and then reconstructed, component by component, to be smooth in the first derivatives and continuous in the second derivatives. A fourth order Runge-Kutta integrator was converted into TPSA integrator using the LBNL version of the TPSA package [9], originally written by Berz and later modified by Etienne Forest. A Taylor map, truncated to second order, was obtained for trajectories starting from the entrance of the Snake .

The spin matrix was obtained by sending three representative trajectories with initial spin conditions as $\vec{S}_o = (S_{xo}, S_{yo}, S_{so}) = (1, 0, 0), (0, 1, 0), (0, 0, 1)$, respectively but with identical initial orbital conditions. Taking the values of spin components at the exit of the Snake, we obtain the spin matrices in the form

$$\begin{bmatrix} S_x \\ S_y \\ S_s \end{bmatrix} = \begin{bmatrix} S_{11} & S_{12} & S_{13} \\ S_{21} & S_{22} & S_{23} \\ S_{31} & S_{32} & S_{33} \end{bmatrix} \begin{bmatrix} S_{xo} \\ S_{yo} \\ S_{so} \end{bmatrix} \quad (2.3)$$

The spin matrix M_S is then expressed as follows.

$$M_S = \begin{bmatrix} S_{x1} & S_{x2} & S_{x3} \\ S_{y1} & S_{y2} & S_{y3} \\ S_{s1} & S_{s2} & S_{s3} \end{bmatrix} \quad (2.4)$$

Note that since the rotation of the spin vector is a subgroup of space rotation, SO(3), the spin precession transformation matrix can also be expressed as follows

$$M_S = \exp(-\theta J_i \cdot \omega_i) = \exp(-\theta \vec{\omega} \cdot \vec{J}) \quad (2.5)$$

where $\vec{\omega}$ is the vector of spin axis and is the normalized eigenvector of the spin matrix M_S . θ is the rotation angle, which can be obtained by calculating the eigenvalues of spin matrix M_S and the J_i s are 3×3 matrices defined as follows:

$$J_1 = \begin{bmatrix} 0 & 0 & 0 \\ 0 & 0 & 1 \\ 0 & -1 & 0 \end{bmatrix}, \quad J_2 = \begin{bmatrix} 0 & 0 & -1 \\ 0 & 0 & 0 \\ 1 & 0 & 0 \end{bmatrix}, \quad J_3 = \begin{bmatrix} 0 & 1 & 0 \\ -1 & 0 & 0 \\ 0 & 0 & 0 \end{bmatrix} \quad (2.6)$$

The angles of the spin axis are defined as (see Fig. 1)

$$\begin{cases} \tan \phi = \frac{\omega_1}{\omega_3} \\ \tan \theta = \frac{\omega_2}{\sqrt{\omega_1^2 + \omega_3^2}} \end{cases} \quad (2.7)$$

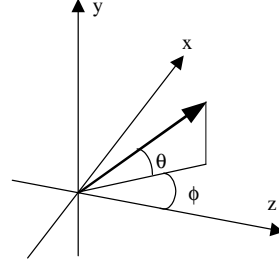


Fig. 1 Angles of the axis of spin precession

In practice, the magnetic field of the Snake is optimized to rotate the spin as completely as possible for a specific energy, typically the injection energy. Since the Snake field remains constant during acceleration, the resultant spin matrices and orbital maps are energy-dependent. These energy dependent matrices and maps can be obtained by interpolation. However, care must be taken not to spoil the symplecticity of the maps as well as the unitary property of the spin matrices. Since the acceleration cycle involves on the order of 10^7 turns, violations of unitary/symplectic conditions larger than 10^{-8} are unacceptable. We first address the issue of symplecticity in the next section. We then discuss how to insert matrices and maps of Snakes into the RHIC lattice.

3. Symplectification of orbital map of the Snake

A $2n \times 2n$ matrix M is said to be symplectic if the matrix M satisfies the condition,

$$M^T \cdot J \cdot M = J, \quad (3.1)$$

where M^T is the transposed of M , and J is defined as

$$J = \begin{bmatrix} 0 & I \\ -I & 0 \end{bmatrix} \quad (3.2)$$

where I is the identity matrix. For a typical 4×4 linear orbital Snake matrix calculated by TPSA using numerically computed magnetic fields, it was found that symplecticity condition violations are on the order of 10^{-4} . These violations can be attributed not only to the truncation process, but also to the fact that numerically calculated magnetic fields do not exactly satisfy Maxwell's equations in the fringing regions. Since the map M (to second order) from the entrance to the exit of the Snake is nearly the map for a drift of length equal to that of the Snake, we can construct a new map M_K as

$$M_K = D^{-1}\left(\frac{L}{2}\right) \cdot M \cdot D^{-1}\left(\frac{L}{2}\right), \quad (3.3)$$

where $D(L/2)$ is a map for a drift half the length of a full Snake, and the linear part of M_K is a near identity matrix which can be written in exponential form [10] as

$$M_K = \exp(\vec{F} \cdot \vec{\nabla}) Id \quad (3.4)$$

where Id is the identity map and $\vec{F} \cdot \vec{\nabla}$ is a Lie operator.

It is obvious that if M_K is symplectic, $\vec{F} \cdot \vec{\nabla}$ should be a Poisson Bracket operator, i.e.,

$$\vec{F} \cdot \vec{\nabla} = :f: \quad (3.5)$$

where f is a function related to \vec{F} .

Then, we can calculate f from \vec{F} by

$$f(\vec{z}) = \int_0^{\vec{z}} J \cdot \vec{F}(\vec{z}') \cdot d\vec{z}' \quad (3.6)$$

where $\vec{z} = (x, p_x, y, p_y, -c\Delta t, p_t)$ is a vector in the phase space. If the map corresponding to \vec{F} is symplectic, then this computation involves an integral of a curl free function and the function f is unique. If the map corresponding to \vec{F} is slightly non-symplectic,

then the function f is one possible symplectification of the vector field \vec{F} and it will depend on the path of the integration. The path length chosen here is the diagonal of the 6-dimensional hypercube, which has one corner at the origin $\vec{z} = (0, 0, 0, 0, 0, 0)$, and an opposite corner at $\vec{z} = (x, p_x, y, p_y, -c\Delta t, p_t)$.

In the present study, a possible symplectic matrix $(M_K)_{\text{symp.}}$ for M_K was computed by an iterative process. Since the computation does not separate the map to be symplectified into the first and second order, it can be used for the symplectification of any order map. Once f is obtained from \vec{F} , the resulting symplectified map for M_K is given as

$$(M_K)_{\text{symp.}} = \exp(:f:)Id \quad (3.7)$$

and

$$(M)_{\text{symp.}} = D\left(\frac{L}{2}\right) \cdot (M_K)_{\text{symp.}} \cdot D\left(\frac{L}{2}\right), \quad (3.8)$$

The details of the symplectification will be published elsewhere [11]. Suffice it to mention that for a typical symplectified linear 4×4 matrix for a Snake at 25GeV violations of the symplecticity condition were found to be less than 10^{-8} .

4. Upgrade of the code SPINK

The general idea of code SPINK [12] is to track a certain number of protons through the machine lattice where matrices are used to transform the orbit and spin coordinates. The orbit matrices are built from a *Twiss* file, output from the code MAD [13]. Since the strength of spin resonances depends on the distance of a particle from the central orbit, misalignments of magnets and field errors must be taken into account. The code MAD was therefore modified to transmit machine element alignment errors and the associated corrected closed orbit and corrector strengths to the code SPINK. Accordingly, SPINK displaces and rotates the orbit maps, and treats correctors as kick magnets on spin motion.

4.1 Insertion of energy dependent orbital maps into RHIC lattice

There are two types of Siberian Snakes in each ring of RHIC. Their function is to rotate the spin by 180° around an axis at 45° with respect to the longitudinal direction s in the x - s plane for Type-A and at -45° for Type-B. Two types of Snake were introduced into RHIC lattice as follows:

$$M = [D_{L/2}][M_{\text{effect}}][D_{L/2}] \quad (4.1)$$

where M represents an orbital map M_T or a spin matrix M_S . M_T is a 6-D symplectified orbital map of the Snake, L is the length of the Snake, $D_{L/2}$ is a drift matrix for a half length Snake. M_{effect} is the thin map for the orbit motion and spin precession. It should be noticed that the map M generally includes a finite zeroth order (dipole) contribution which would perturb the closed orbit as computed by MAD. This is especially true in the low energy region below 100 GeV, although the deviations are quite small. Since the net dipole contributions from the Snakes errors would be normally taken into account by the closed orbit correction procedure, they are simply zeroed here.

4.1.1 Interpolation of orbital map

We obtained the symplectic orbital maps of the Snake by extracting the potential candidates \mathcal{F} for the Poisson bracket operator from a single vector field representation \vec{F} as shown in Eq.(3.7). To guarantee the symplecticity of the interpolated map, the Poisson bracket operator \mathcal{F} (rather than the map itself) was pre-calculated at every 0.5GeV from 25GeV to 250GeV and interpolated.

4.1.2 Interpolation of spin matrices

The orthogonal 3×3 spin matrix consists of 9 elements. The spin matrix at the energy E between E_i and E_{i+1} ($i=1, 2, \dots, n$) could be obtained simply by interpolating each of the elements of the spin matrices at E_i and E_{i+1} . However, it was found that the unitarity of spin matrices interpolated in this way can not be guaranteed. Actually, spin polarization was totally lost after 10,000 turns of tracking with thus obtained spin matrices.

For this reason, we developed a new method of interpolating spin matrices. Since the rotation of spin is a subgroup of the space rotation $SO(3)$, a spin matrix can be described completely using a smaller number of parameters i.e. the three components of vector $\vec{v} = (v_1, v_2, v_3) = -\theta \vec{\omega}$ as is given in Eq.(2.3). Interpolation of the spin matrix with respect to vector \vec{v} can be done as follows: First, by calculating the eigenvalues and eigenvectors of the matrix of $M_s(E_i)$, we obtain the rotation angle θ and the normalized eigenvector $\vec{\omega}$, and then $\vec{v} = \theta \vec{\omega}$. We then store the three components of the vector

$$\vec{v}(E_i) = [v_1(E_i), v_2(E_i), v_3(E_i)], \quad i = 1, 2, \dots, n \quad (4.2)$$

at energy E_1, E_2, \dots, E_n from the injection energy of 25GeV to the top energy of 250GeV with uniform step $\Delta E (= 0.5 \text{ GeV})$. Then, we interpolate the three elements of the vector \vec{v} at the energy E , which is between E_i and E_{i+1} . Finally, the spin matrix can be recalculated by Eq. (2.3.3) and its unitarity is guaranteed by construction.

4.2 Symplectification of orbit maps provided by MAD

The orbital tracking was done with use of orbital maps of all the elements in RHIC lattice obtained from code MAD, which is not a long term tracking code. The symplecticity of these orbital maps was therefore checked. Although the maximum symplecticity violation for a single element was 9.57×10^{-8} , the violation for a One Turn Map (OTM) obtained by concatenating all elements, except Siberian Snakes, is 5.6×10^{-6} in (x, p_x) phase space and 4.5×10^{-9} in (y, p_y) phase space. Obviously, this is not accurate enough for tracking over 10^7 turns.

It is known that a matrix M can be written in exponential form

$$M = \exp(B) \quad (4.3)$$

where B is a real matrix. The Cayley representation [10] of M is given as

$$M = (I + T)(I - T)^{-1} = (I - T)^{-1}(I + T), \quad (4.4)$$

where $T = \tanh(B/2)$. Let's define a symmetric matrix W by taking the symmetric part of V , $V = J^{-1} T$, as follows:

$$W = (V + V^T) / 2 \quad (4.5)$$

then, we define a symplectic matrix R by writing

$$R = (I + JW)(I - JW)^{-1} = (I - JW)^{-1}(I + JW), \quad (4.6)$$

R will be a symplectification of M that we call the Cayley symplectification. The first order matrices of the elements in RHIC lattice were symplectified by this method, and the symplecticity of matrices is guaranteed to be up to machine (computer) precision.

5. Spin Tracking with “Real” Siberian Snakes in RHIC

Armed with energy-dependent unitary spin matrices and symplectified orbital maps, we are now in position to track from injection to top energy. In this section, typical results of such long-term tracking will be presented for different conditions. For single particle tracking, the “emittance” of a particle is defined as the area enclosed by the invariant phase ellipse contour. For multi-particle tracking, the tracked particles are assumed to be Gaussian distributed inside the phase space volume. Each particle is tracked during the course of acceleration from the injection energy 25GeV to the top energy 250GeV. The momentum gain per turn is assumed to be 3×10^{-5} (GeV/c). Although there are 5 RF cavities in each RHIC ring,

only two of them are used for acceleration of polarized proton. Each cavity has a peak voltage of approximately 300 KV. The acceleration time is 80 seconds, which corresponds to a total of 7.5×10^6 turns.

5.1 Spin tracking with ideal Siberian Snakes

We first consider the case where the Siberian snakes are ideal, i.e. where the orbital map is identity and the spin matrices are as follows:

$$M_{s_Type_A} = \begin{bmatrix} 0 & 0 & 1 \\ 0 & -1 & 0 \\ 1 & 0 & 0 \end{bmatrix} \quad M_{s_Type_B} = \begin{bmatrix} 0 & 0 & -1 \\ 0 & -1 & 0 \\ -1 & 0 & 0 \end{bmatrix}$$

for Type-A: the spin axis is in the x - s plane and for the Type-B: the spin axis is in the x - s plane.

Fig. 2 shows spin depolarization for particles with a normalized emittance 5π mm-mrad, 10π mm-mrad, 15π mm-mrad and 20π mm-mrad, respectively. The normalized polarization, horizontal and vertical amplitudes are plotted against $G\gamma$, which is proportional to the energy. Symplectified orbital maps are used; misalignment and field errors are not included. It is well known [14] that the intrinsic resonances are enhanced at $G\gamma = mP \pm \nu_y$ where P is the superperiodicity of the lattice, ν_y is the vertical betatron oscillation frequency and m is an integer. Intrinsic resonances are also enhanced at $G\gamma = mPM \pm \nu_B$ where M is the number of FODO cells, and ν_B is the total accumulated phase advance in dipole cells [15]. The enhancement due to M is important because normally $M \gg P$ in high energy accelerators; furthermore, dominant resonances are located at m =odd integers since in that case spin kicks due to the focusing and defocusing quadrupoles add up coherently.

Fig. 2 shows three strong depolarization resonances occurring at $(G\gamma)_1 = 3 \times 81 - (\nu_y - 12) = 225.82$, $(G\gamma)_2 = 3 \times 81 + (\nu_y - 12) = 260.18$, and $(G\gamma)_4 = 5 \times 81 + (\nu_y - 12) = 422.18$, where 81 is the product of the superperiodicity $P=3$ and the “effective” FODO cells per superperiod $M=27$ (which includes the dispersion suppressors) and $2\pi\nu_B = 2\pi(\nu_y - 12)$ is the accumulated phase advance of all FODO cells. A fourth strong depolarizing resonance is found at the location $(G\gamma)_3 = 5 \times 81 - (\nu_y - 6) = 381.82$.

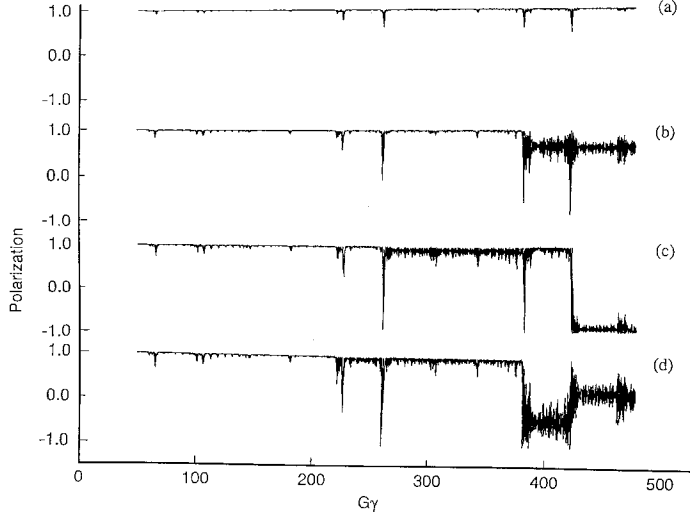


Fig. 2 Spin tracking with perfect Snakes in RHIC, orbit tracking with symplectified matrices

- a.* $\varepsilon_x = \varepsilon_y = 5\pi\text{mm}\cdot\text{mrad}$, *b.* $\varepsilon_x = \varepsilon_y = 10\pi\text{mm}\cdot\text{mrad}$,
c. $\varepsilon_x = \varepsilon_y = 15\pi\text{mm}\cdot\text{mrad}$, *d.* $\varepsilon_x = \varepsilon_y = 20\pi\text{mm}\cdot\text{mrad}$.

5.2 Spin tracking with real Siberian Snakes

5.2.1 Intrinsic resonances

We now present results of long-term tracking performed with Siberian Snake maps derived from three-dimensional numerical field computations and symplectified using the technique previously described. Fig. 3 presents the result of single particle tracking assuming no misalignments and no field errors. Therefore, the depolarization resonances are intrinsic resonances. Comparing with the results in Fig. 2, we find that “real” snakes maintain the polarization better than idealized snakes. With idealized snakes, the polarization can not be recovered after crossing the resonance at $(G\gamma)_3 = 381.82$ and decreases to 88% for particles with emittance larger than 10π mm-mrad. Using realistic snakes, polarization can be maintained to 95% under the same conditions.

Realistic snakes introduce coupling that is not present with idealized ones. This can be seen by observing betatron amplitudes in the x and y directions at a specific location where $\beta_{T_x} = 9.956\text{m}$, $\beta_{T_y} = 10.044\text{m}$. Due to adiabatic damping, the x and y amplitudes decrease with acceleration. With real snakes, the amplitudes in x plane and y plane are exchanged, shown in the left and right plots of Fig. 4, indicating the presence of coupling. The effect is most noticeable in

the low energy region ($G\gamma < 150$) since the source of transverse coupling in “real” Siberian Snakes is the longitudinal component of the fringe field. The initial emittance is $5\pi\text{mm-mrad}$.

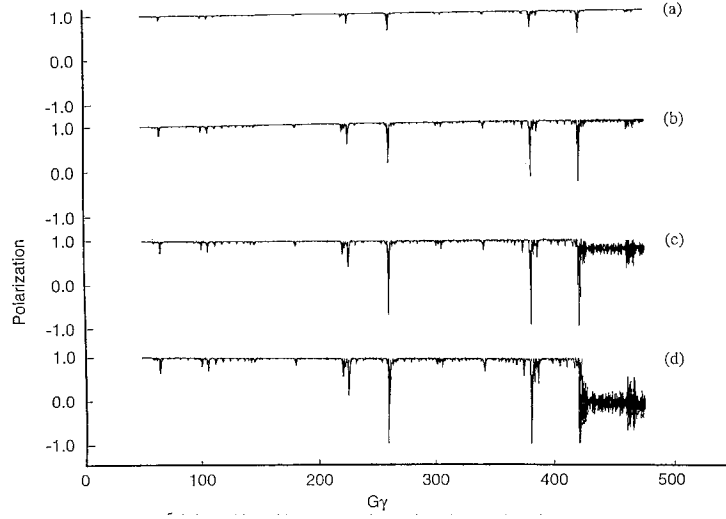


Fig. 3 Spin tracking with real Snakes in RHIC, orbital tracking with the symplectified matrices from Code MAD.

- a.* $\epsilon_x = \epsilon_y = 5\pi\text{mm-mrad}$, *b.* $\epsilon_x = \epsilon_y = 10\pi\text{mm-mrad}$,
c. $\epsilon_x = \epsilon_y = 15\pi\text{mm-mrad}$, *d.* $\epsilon_x = \epsilon_y = 20\pi\text{mm-mrad}$.

Coupling induces a change in betatron tunes. We calculated these tunes from the eigenvalues of the One Turn Map (OTM), obtained by concatenating all the element matrices in the lattice, as well as the two Siberian Snakes' maps. In Fig. 5, the betatron tunes are shown as a function of

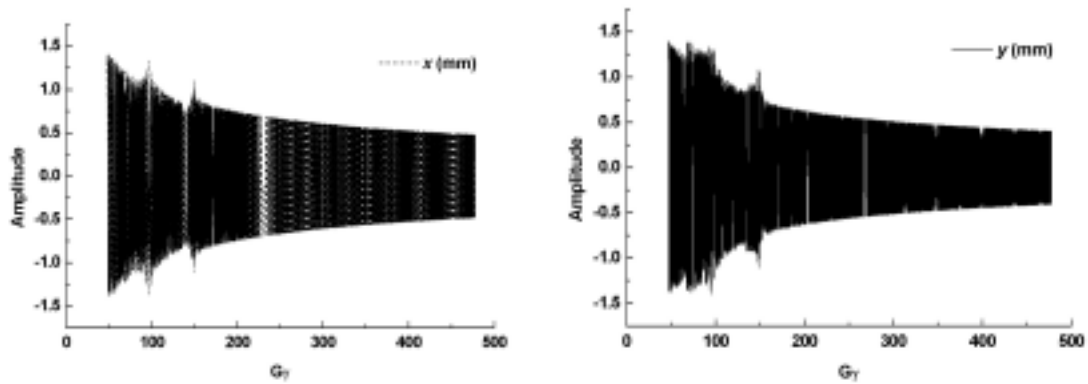


Fig. 4 Betatron amplitude in x and y plane at 6'oclock in the RHIC ring.

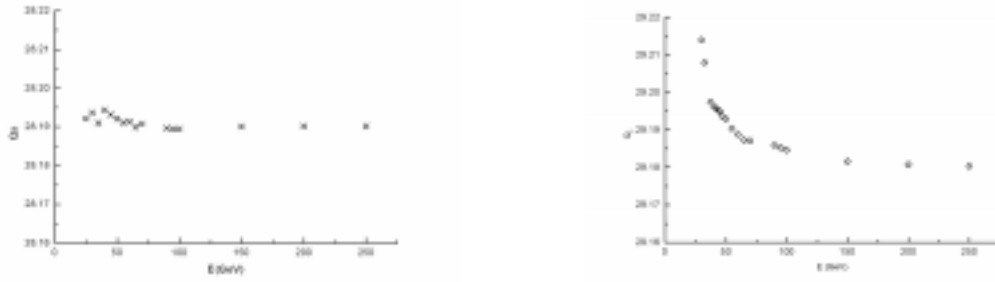


Fig. 5 The transverse betatron tunes Q_x and Q_y shifts through the acceleration

proton energy. The maximum tune shifts from the designed working points are $\Delta Q_x=0.01919$ and $\Delta Q_y =0.0306$ at injection energy (25GeV). Fig 6 is a tune diagram where tunes at different energies are marked with circles and the design working point $Q_x = 28.19$ and $Q_y =29.18$ is marked with a triangle. In this diagram, neighboring sum resonances $nQ_x + mQ_y = p$, are illustrated as well as difference resonances $Q_x - Q_y =-1$ where n, m and p are positive integers and $n+m$ denotes the order of the resonances. The RHIC design tune is located between the 5th order resonance at 28.20 and the 6th order resonance at 28.166, making the usable range approximately 0.034. As the energy is increased, the tunes gradually move toward the design working point and cross the 5th and 10th order sum resonances ($G\gamma \sim 71.67$) causing an increase in betatron amplitudes. In the energy region from 45 GeV to 70 GeV ($G\gamma$ from 86.01 to 133.79), the tunes cross the difference resonance $Q_x - Q_y =-1$. Difference resonances cause amplitude exchange but do not induce further amplitude growth. Since spin resonance strengths are proportional to $G\gamma$, spin motion is not seriously damaged by larger betatron amplitudes in the low energy region.

5.2.2 Intrinsic and imperfection resonances

Imperfection resonances arise from magnet misalignments. Misalignments were assigned randomly to magnets in all FODO arc cells assuming a truncated Gaussian distribution. The effects of these misalignments as well as those of the closed orbit correction system on the spin motion are investigated. Two categories of simulation were carried out:

Category 1:

In this category, the effects of vertical closed orbit correctors are investigated. These correctors have horizontal magnetic fields, and it is anticipated that the depolarization will be large when the correction is strong. The standard deviation (σ) of the Gaussian dipole magnet misalignment distribution is set to be 0.1mm, 0.5mm, 1.0mm and 2.5mm, in both the horizontal

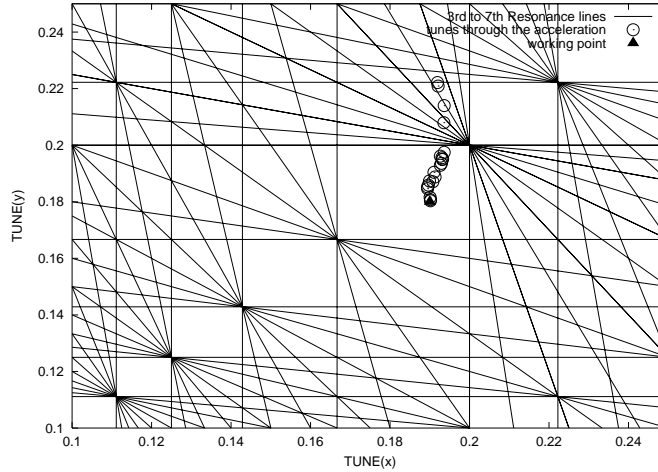
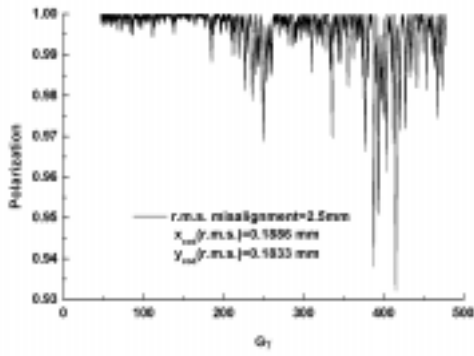


Fig.6 Tune diagram showing the selected working point of RHIC at $Q_x = 28.19$ and $Q_y = 29.18$ (with symbol “▲”) with neighboring sum and difference resonances. The shifted working point due to the insertion of Snakes are shown with symbol “○” in the diagram.

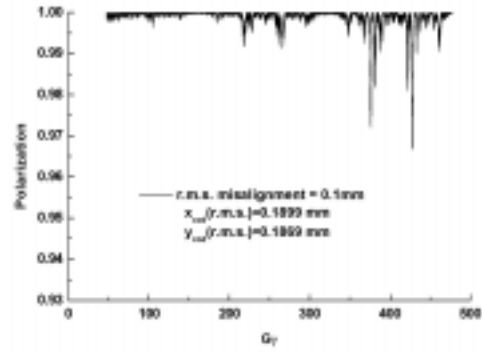
and vertical planes. In addition, the corresponding value of σ for the main dipoles roll angle is 1 mrad. For the main quadrupoles (QF, QD) and sextupoles the rms offsets are set to 1 mm in both planes. The closed orbit distortions were corrected to 0.180 mm (r.m.s.) using the Micado procedure[MICADO], and the tunes were kept at 28.19 (H) and 29.18 (V) by adjusting the quadrupoles' strengths in the arc cells. Single-particle tracking was done for a particle of zero emittance $\epsilon_x = \epsilon_y = 0$. In this case, depolarization is mainly due to imperfections resonances. Tracking results are given in Figs. 7 (a), (b), (c) and (d), respectively. In these figures, one can see that depolarization increases with the magnitude of the misalignments, reflecting the effect of the correctors on spin motion. For a given rms amplitude of the corrected closed orbit error, the corrector strengths increase with the misalignments. The transverse fields associated with both the magnet misalignments and the correctors result in a stronger perturbation of the spin motion.

Category 2:

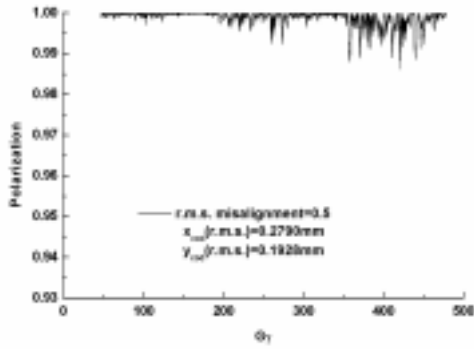
In this case, the standard deviations for main dipoles offset and roll are set to 2.5 mm and 1 mrad respectively. The r.m.s offset of the main quadrupoles (QF, QD) and sextupoles are set to 1 mm in both planes. Using Micado algorithm, the vertical closed orbit distortion was corrected to 0.189 mm (r.m.s.) and 0.512mm (r.m.s.). The tunes Q_x and Q_y are kept 28.19 (H) and 29.18 (V), by adjusting the arc cell quadrupoles. Single particle spin tracking was performed for particles with emittance 5π mm-mrad, 10π mm-mrad, 15π mm-mrad and 20π mm-mrad, respectively. The results are presented in Fig. 8.1 and Fig. 8.2 for corrected closed orbit distortion of 0.189 mm and



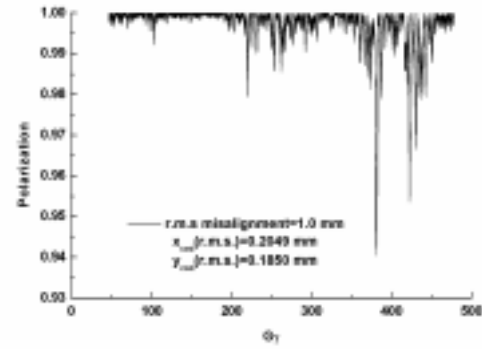
(a)



(b)



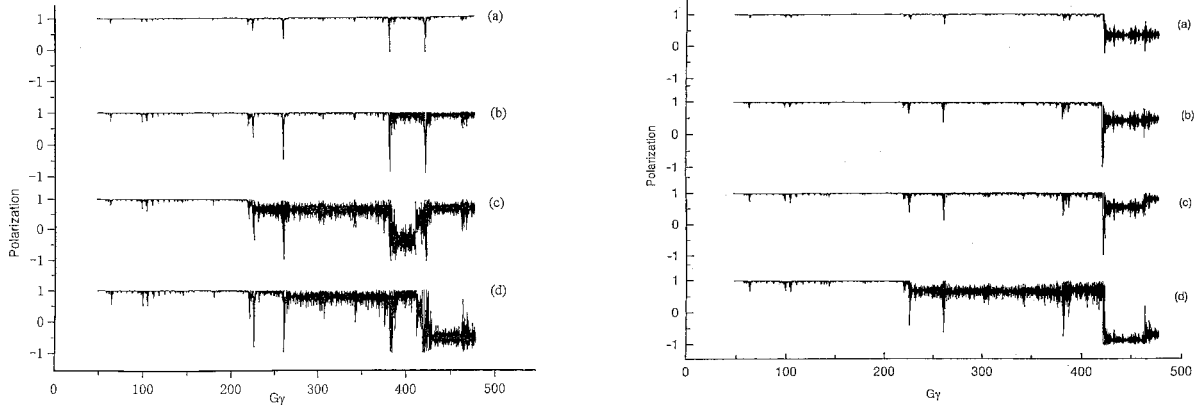
(c)



(d)

Fig 7 The effect of the misalignments of RHIC on spin motion. Spin tracking was done by single particle extracted from the emittance of zero. Corrected vertical closed orbit distortions $\approx 0.18\text{mm}$. Original r.m.s. misalignments are (a) 0.1mm, (b) 0.5mm, (c) 1.0mm, and (d) 2.5mm

0.512mm respectively. In these figures, depolarization is seen to be more serious due to the presence of both intrinsic and imperfection resonances. It is known that the tolerable imperfection resonance strength decreases dramatically due to the overlapping effect of two types of resonances [16]. For a closed orbit distortion corrected to 0.189mm (r.m.s.), the imperfection resonance strength is less than 0.07 -about 6 times less than the intrinsic resonance strength, and the polarization can still be kept at 88% for an emittance of $10\pi\text{mm-mrad}$. On the other hand, when the corrected closed orbit distortion is 0.5mm, the polarization drops to 36% for an emittance of $5\pi\text{mm-mrad}$, and to 44% for $10\pi\text{mm-mrad}$ case.



(1) Corrected closed orbit distortion ≈ 0.2 mm (2) Corrected closed orbit distortion ≈ 0.5 mm

Fig 8 Spin tracking with real Snakes in RHIC, orbital tracking with the symplectified

matrices from Code MAD. Misalignment randomly assigned,

- a.* $\epsilon_x = \epsilon_y = 5\pi\text{mm-mrad}$, *b.* $\epsilon_x = \epsilon_y = 10\pi\text{mm-mrad}$,
c. $\epsilon_x = \epsilon_y = 15\pi\text{mm-mrad}$, *d.* $\epsilon_x = \epsilon_y = 20\pi\text{mm-mrad}$.

5.3 Multi – particle tracking results

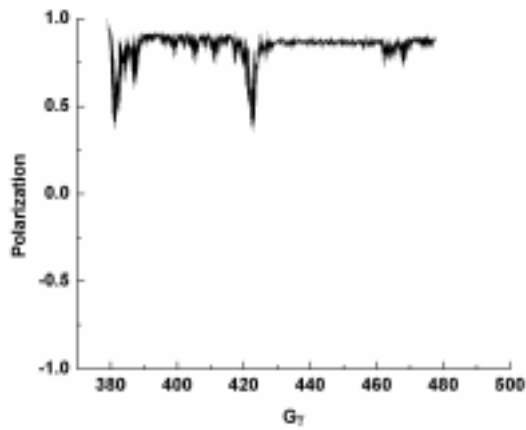
Multi – particle tracking is performed with 32 particles randomly distributed in transverse phase space assuming a Gaussian distribution. We observe from single particle tracking results two strong depolarization resonances happening at $G\gamma=381.82$ and $G\gamma= 422.18$. Therefore, particles are not tracked with acceleration from the injection energy, but rather from 197.92 GeV ($G\gamma=378.18$) to the top energy of 250 GeV ($G\gamma= 477.67$). A r.m.s. emittance of $10\pi\text{mm-mrad}$ is assumed for the ensemble.

The r.m.s. polarization is calculated as follows:

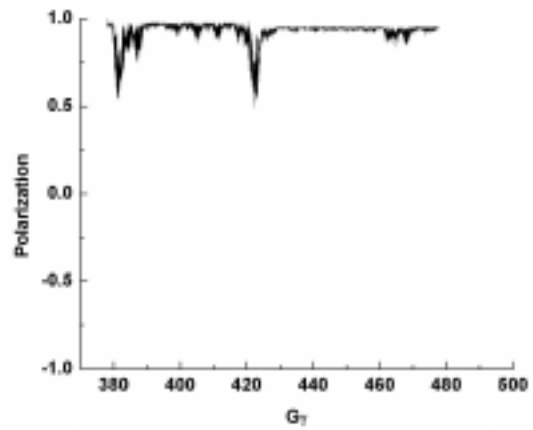
$$S_y(r.m.s.) = \frac{1}{N} \sqrt{\sum_N S_y^2}$$

where N is the number of particles, S_y is the polarization of each particle during the acceleration. First, we compare perfect Siberian Snakes with “real” Siberian Snakes assuming the RHIC lattice without misalignments. Fig. 9a and Fig. 9b show the resulting r.m.s. polarization. Strong depolarizing resonances occur around $G\gamma= 411 - v_y = 381.82$ and $451 - v_y = 421.82$. Perfect

snakes can preserve 88.9% of the average and 87.7% of r.m.s. polarization at the top energy of 250 GeV. In contrast, the corresponding figures for “real” Siberian Snakes are 96.25% and 94.65%. These results are consistent with those obtained from single-particle tracking.



a) with “perfect” snakes in RHIC



(b) with “real” snakes in RHIC

Fig 9 The average results of polarization from the tracking of 32 particles in RHIC with No misalignment and no field errors. Original emittance: $10\pi\text{mm-mrad}$.

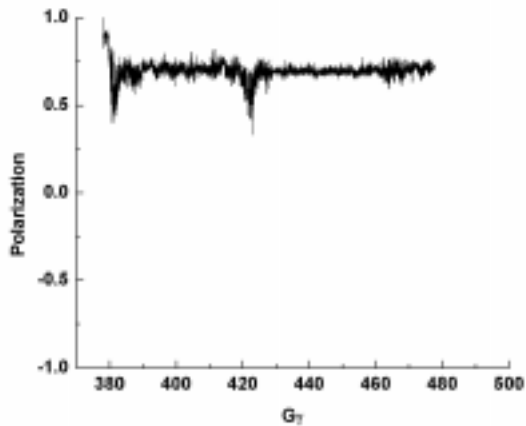


Fig 10 The average results of polarization from the tracking of 32 particles in RHIC with r.m.s. misalignment of 2.5mm and corrected vertical closed orbit distortion of 0.189mm. Original emittance: $10\pi\text{mm-mrad}$.

We also considered real snakes in conjunction with 2.5 mm r.m.s. misalignments and a vertical corrected closed orbit distortion of 0.189 mm. The results are presented in Fig. 10; and the spin polarization drops to 63.1% (average) and 73.0% (rms), as expected.

6. Conclusions

Siberian Snakes are installed in the RHIC ring as local spin rotators to prevent depolarization during acceleration from 25 GeV to 250 GeV. These Snakes are composed of super-conducting helical dipole magnets. The field distribution calculated with the 3D magnetostatics code TOSCA was found to be in close agreement with measurements performed on a prototype magnet. This result motivated tracking studies based on numerically obtained field maps to predict polarization for several accelerator conditions.

To obtain reliable results, the unitarity of spin matrices and the symplecticity of the orbital maps should be guaranteed. Orbital maps obtained by straightforward application of the TPSA approach exhibit violations of the symplectic condition of the order 10^{-4} . This is caused not only by truncation of high order terms but also by the non-Maxwellian character of the numerically obtained magnetic field. We have developed procedures to symplectify numerical maps. Using these procedures, we have produced Siberian Snakes orbital maps symplectic to machine (computer) precision as well as spin matrices for which deviation from unitarity is smaller than 10^{-8} .

We performed long-term spin tracking in the RHIC lattice with maps based on realistic fields obtained from 3D computations. The effects of corrector magnets for vertical closed orbit corrections have been investigated. If the misalignments are large, the strengths of corrector magnets must be strong to make the closed orbit values reasonably small. The important conclusion is that the misalignments should be as small as 0.2 mm when the emittance is less than $10 \pi \text{mm-mrad}$. It is shown that the polarization can be kept with “real” Siberian Snakes in RHIC to more than 95% through acceleration for an ideal machine without imperfection resonances. When the latter are included, the polarization drops to 88% assuming misalignments of 0.1 mm and a closed orbit distortion corrected to less than 0.2mm (r.m.s).

References

- [1] Ya.S.Derbenev et al., Part. Accel. Vol. 8, 115(1978).
- [2] A.U.Luccio, Polarized Protons tracking in the AGS and RHIC. Polarized Protons at High Energy Accelerator Challenges and Physics Opportunities Workshop. BNL 1999.
- [3] H. Wu, et al., *The Spin Tracking Study in RHIC for Polarized Proton*. Brookhaven National Laboratory, AGS/RHIC/SN No. 026.
- [4] J. P. Blewett and R. Chasman, J. Ap. Physics., 48(1977)2692.
- [5] M. Okamura, The Hall Probe Measurement and Calculation of the Half Length Helical Dipole Magne. BNL Spin Note: AGS/RHIC/SN No. 60, August 20, 1997.
- [6] V. Bargmann, Louis Michel and V. L. Telegdi, Precession of the Polarization of Particles Moving in a Homogeneous Electromagnetic Field. Physical Review Letters, Vol. 2, No. 10. P.435.(1995).
- [7] M.Xiao, Spin Dynamics of Polarized Proton Beams in Relativistic Heavy Ion Colliders(RHIC), Ph.D Thesis. Appendix A. December 21, 1999.
- [8] F.Willeke, Modern Tools For Particle Tracking.CAS Fifth Advanced Accelerator Physica Courese, Greace, Sep. 20-Oct.1,1993
- [9] E. Forest, Overloading of Trucated Power Deries Algebra(TPSA). <http://bc1.lbl.gov/CBP-pages/educational/TPSA-DA/introduction.html>.
- [10] A.J.Dragt , Lectures on Nonlinear Orbit Dynamics. AIP Conf. Proc., P.147-313, 1987.
- [11] M.Xiao et al., Field Map Generated Numerical Spin Matrices and Orbital Maps of Siberian Snake for Spin Tracking in RHIC. To be submitted.
- [12] A. Luccio, Numerical Spin Tracking in a Synchrotron. Computer Code SPINK. Examples(RHIC). Brookhaven National Laboratory, AGS/RHIC/SN No. 011.
- [13] Hans Grote and F. Christoph Iselin, The MAD Program(Methodical Accelerator Design) Version 8.13/8 User's Reference Manual. Geneva, Switzerland. January 18, 1994.
- [14] S. Y. Lee, Spin Dynamics and Snakes in Synchrotrons. Indiana University, Bloomington; USA. World Scientific Publishing Co. Pte. Ltd. Chapter 3, P25-42, 1997.
- [15] T. Roser a el., Design Manual, Polarized Proton Collider at RHIC. Brookhaven National Laboratory, July 1998.
- [16] S.Y. Lee, *Prospects for Polarization at RHIC and SSC*, Polarized Collider Workshop, AIP Conference Proceeding Vol. 223, P₃₀,1990.